Exceptionally Short Tetracoordinated Carbon–Halogen Bonds in Hexafluorodihalocubanes

Masafumi Sugiyama,[1] Yuta Uetake,[2,3*] Nozomu Miyagi,[4] Masaaki Yoshida,[4,5] Kyoko Nozaki,[1] Takashi Okazoe,[1,6] and Midori Akiyama[7*]

[1]Department of Chemistry and Biotechnology, Graduate School of Engineering, The University of Tokyo, Bunkyo-ku, Tokyo 113-0032, Japan

[2]Department of Applied Chemistry, Graduate School of Engineering, Osaka University, Suita, Osaka 565-0871, Japan

[3]Innovative Catalysis Science Division, Institute for Open and Transdisciplinary Research Initiatives (ICS-OTRI), Osaka University, Suita, Osaka 565-0871, Japan

[4]Department of Applied Chemistry, Graduate School of Sciences and Technology for Innovation, Yamaguchi University, Ube, Yamaguchi 755-8611, Japan

[5]Blue Energy Center for SGE Technology (BEST), Yamaguchi University, Ube, Yamaguchi 755-8611, Japan

[6]AGC Inc., Suehiro-cho, Tsurumi-ku, Yokohama, Kanagawa 230-0045, Japan

[7]Department of Molecular Engineering, Graduate School of Engineering, Kyoto University, Kyoto-shi, Kyoto 615-8510, Japan

ABSTRACT: Molecules that contain bonds whose length significantly deviates from the average are of interest in the context of understanding the nature and limits of chemical bonds. However, it is difficult to disentangle the individual contributions of the multiple factors that give rise to such bond-length deviations, as reports on such molecules remain scarce. In the present study, we have succeeded in synthesizing hexafluorodihalocubanes of the type $C_8F_6X_2$ (**2**) (X = Cl (**2**$_{Cl}$), Br (**2**$_{Br}$), I (**2**$_{I}$)), which represent a new series of molecules with unusual C(sp^3)–halogen bonds. The C(sp^3)–halogen bonds of **2**$_{Cl}$, **2**$_{Br}$, and **2**$_{I}$, determined via single-crystal X-ray diffraction analysis, are by approximately 0.07–0.09 Å shorter than typical C(sp^3)–halogen bonds. In particular, the carbon–iodine bonds of **2**$_{I}$ are the shortest C(sp^3)–I bonds reported to date. The solution-state structures and electronic states of the C(sp^3)–halogen bonds in these hexafluorodihalocubanes were analyzed by X-ray absorption spectroscopy, which revealed detailed information on the length of these C(sp^3)–halogen bonds in solution and the solid state as well as on the electron-accepting nature of **2**. Detailed theoretical calculations and a comparison with halotrinitromethanes (**1**), which represent another series of molecules with shortened C(sp^3)–halogen bonds, revealed that the factors responsible for the shortening of the C(sp^3)–halogen bond vary among the different C(sp^3)–halogen bonds, i.e., for C(sp^3)–Cl and C(sp^3)–Br, the s-character and hyperconjugation effects predominate, whereas for C(sp^3)–I, the interatomic Coulombic interaction effect prevails.

Introduction

Chemical bonds link atoms to form molecules. The limits of bond lengths have long been studied in order to understand the nature of chemical bonds.[1,2] Although the length of a chemical bond rarely diverges significantly from the average for that bond type,[1,3–5] the synthesis of molecules with significantly shortened[6,7] or elongated bonds[4,8–17] has been achieved. The present study focuses on C(sp^3)–halogen bonds (C(sp^3)–Cl, C(sp^3)–Br, C(sp^3)–I), a fundamental class of bonds in organic compounds, that are exceptionally short. It should be noted here that a C–halogen bond on a tetracoordinated carbon atom may not comprise a pure sp^3-hybridized carbon orbital, but instead an orbital with relatively high s-character, especially when the bond is short. However, in the interest of simplicity, the tetracoordinated carbon atoms are denoted as C(sp^3) in this paper. Historically, halotrinitromethanes (**1**; X = Cl (**1**$_{Cl}$), Br (**1**$_{Br}$), and I (**1**$_{I}$)) have been studied as molecular frameworks for shortened C(sp^3)–halogen bonds.[18,19] Their C(sp^3)–halogen bonds were found to be much shorter than the average based on single-crystal X-ray and gas-electron diffraction analyses (**Figure 1A, B**). In general, the following factors have been proposed to cause the shortening of atom–atom bonds: 1) higher s-character for each atom,[20] 2) hyperconjugation and multiple-bond character,[21] and 3) interatomic Coulombic interactions.[22] However, it is difficult to comprehensively disentangle the contributions of each of these factors to the overall bond shortening. A comparison of the halotrinitromethane (**1**) series with another series of compounds with shortened C(sp^3)–halogen bonds can be expected to provide greater detail, albeit that reports of examples other than **1** remain scarce[23–27] (**Figure 1C**). A common feature of these sporadic examples is that they contain a strained backbone and/or electron-deficient groups.

In this context, we focused on the polyfluorocubane skeleton, which has recently been synthesized in our group.[28] Polyfluorocubanes are strained and electron-deficient, and accordingly, we anticipated that introducing halogen atoms into these molecules would lead to shortened C(sp^3)–halogen bonds.

In the present study, we succeeded in synthesizing a series of hexafluorodihalocubanes of the type $C_8F_6X_2$ (**2**) (X = Cl (**2**$_{Cl}$), Br (**2**$_{Br}$), I (**2**$_I$)) and investigated their bond lengths using single-crystal X-ray diffraction (scXRD) analysis and X-ray absorption spectroscopy (XAS) (**Figure 1D**). As predicted, the C(sp^3)–halogen bonds of **2** are shorter than average, and in particular, **2**$_I$ exhibits the shortest C(sp^3)–I bond reported to date. A comparison of the bond lengths of **2** with those of the hitherto reported series of halotrinitromethanes (**1**) revealed that the Cl and Br analogues of **1** exhibit shorter C(sp^3)–halogen bonds, while in the case of the iodine analogues, **2**$_I$ exhibits a shorter bond. DFT calculations were used as the basis of a comprehensive discussion of each of the contributing factors to the overall bond shortening.

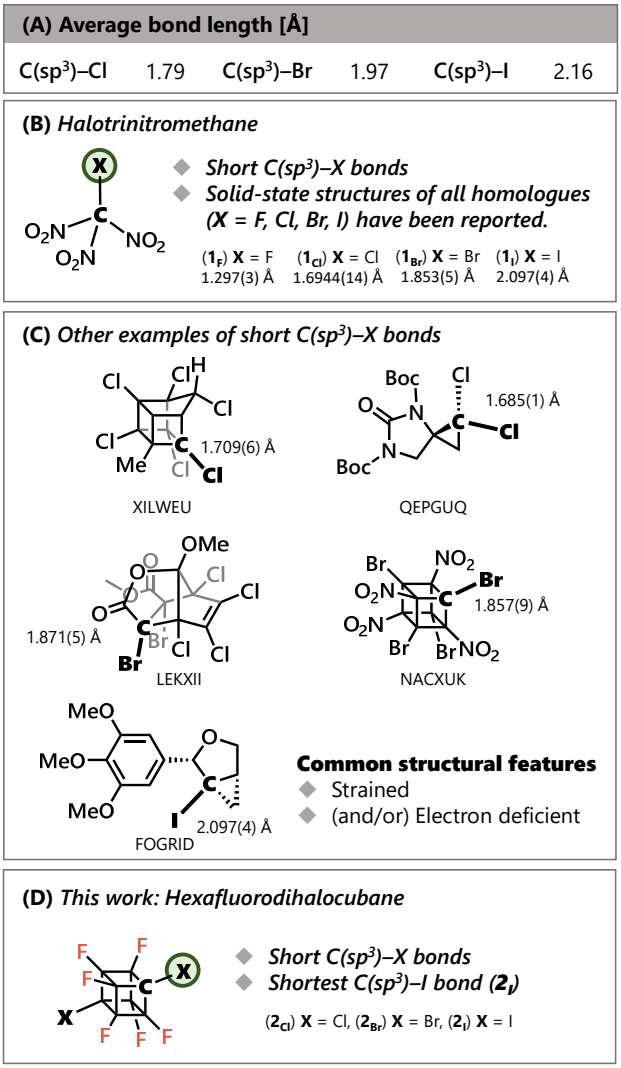

Figure 1. Examples of compounds with short C(sp^3)–halogen bonds and their experimentally determined bond length. (A) Average lengths of C(sp^3)–halogen bonds. (B) Halotrinitromethanes. (C) Examples of other compounds than halotrinitromethanes with short C(sp^3)–halogen bonds. The CSD reference code is noted below each structure. (D) Hexafluorodihalocubanes (*this work*).

Results and Discussion

Synthesis of hexafluorodihalocubanes (2). The synthetic route to hexafluorodihalocubanes (**2**) is shown in **Scheme 1**. Hexafluorocubane (**3**)[28] was deprotonated in THF using lithium bis(trimethylsilyl)amide (LiHMDS) and subsequently treated with the corresponding aryl sulfonyl halides to generate hexafluorodihalocubanes **2**$_{Cl}$, **2**$_{Br}$, and **2**$_I$.[29,30] After the reactions, the solvent was removed by distillation and compounds **2** were isolated via sublimation. All compounds are solids and stable under an ambient atmosphere and temperature. The structures of **2** in the solid state and in solution were unambiguously determined using ^{19}F NMR and ^{13}C{^{19}F} NMR spectroscopy as well as scXRD analysis. The ^{19}F NMR spectra of **2** feature one singlet each, whose chemical shift moves to lower field with increasing atomic number of the substituted halogen atom (**2**$_{Cl}$: –187.99 ppm, **2**$_{Br}$: –182.50 ppm, **2**$_I$: –173.08 ppm).

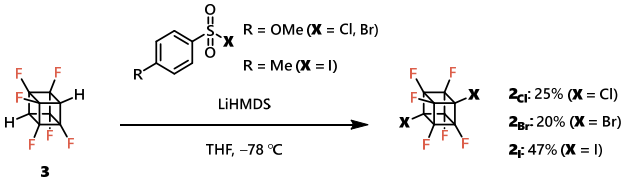

Scheme 1. Synthesis of hexafluorodihalocubanes 2$_{Cl}$**, 2**$_{Br}$**, and 2**$_I$**.**

Crystal-structure analysis of hexafluorodihalocubanes (2). The solid-state structures and metric parameters for **2**$_{Cl}$, **2**$_{Br}$, and **2**$_I$, obtained from the scXRD analyses are shown in **Figure 2**. Each hexafluorodihalocubane exhibits slightly distorted D_{3d} symmetry, and the variances in the C–C and C–F bond lengths are within 0.01 Å. In addition, the C(sp^3)–halogen bonds of **2**$_{Cl}$, **2**$_{Br}$, and **2**$_I$ are by approximately 0.07–0.09 Å shorter than the corresponding typical C(sp^3)–halogen bonds.[3]

To investigate how significant the shortening of these bonds is, we analyzed the Cambridge Crystal Structure Database (CCSD) (**Figure 3**); for detailed search criteria, see the Supporting Information. The obtained results show that **2** exhibit extremely short C(sp^3)–X bonds, ranking within the top 1% of the CCSD. In particular, the carbon–iodine bonds of **2**$_I$ are the shortest C(sp^3)–I bonds among hitherto reported examples satisfying the defined criteria. Interestingly, a comparison of the bond lengths of **1** and **2** revealed that the C(sp^3)–Cl and the C(sp^3)–Br bonds are shorter in **1**, while the C(sp^3)–I bonds are shorter in **2** (**Table 1**). This result suggests that the magnitude of the contributions of the different factors associated with bond shortening vary even among homologous halogen–carbon bonds. It should be noted here that perfluorocubane can be regarded as the corresponding fluorine-substituted hexafluorodihalocubane.[28] However, a fair comparison is difficult due to the different symmetry of this molecule (O_h). Therefore, a comparison of the C–F bond lengths in perfluorocubane and fluorotrinitromethane (**1**$_F$) has been excluded from this study. Regardless, the C–F bond lengths of perfluorocubane are 1.3406(17) and 1.338(3) Å in the solid state, which are shorter than the average C–F bond (1.40 Å), but longer than that of **1**$_F$ (1.297(3) Å).[19]

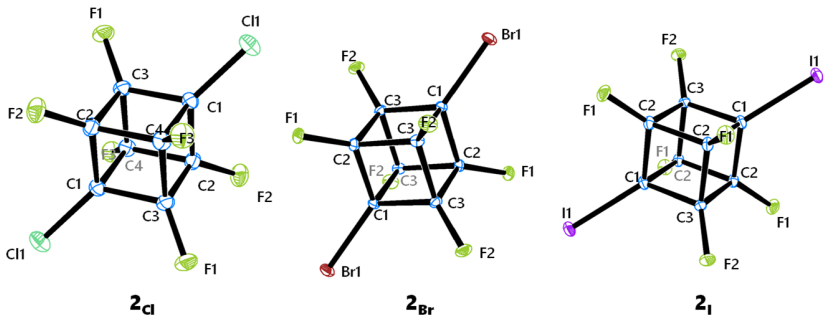

Bond length [Å]			
	2_{Cl}	2_{Br}	2_{I}
C–X	Cl1–C1 1.7170(18)	Br1–C1 1.878(3)	I1–C1 2.079(3)
C–F	F2–C3 1.345(2) F3–C4 1.344(2) F1–C3 1.335(2)	F1–C2 1.346(3) F2–C3 1.337(2)	F1–C2 1.343(3) F2–C3 1.342(3)
C–C	C4–C3 1.574(2) C4–C2 1.575(2) C4–C1 1.569(3) C3–C2 1.564(3) C3–C1 1.568(2) C2–C1 1.573(2)	C1–C2 1.565(3) C1–C3 1.567(2) C3–C3 1.575(3) C2–C3 1.570(2)	C1–C2 1.571(3) C1–C3 1.569(4) C2–C2 1.568(4) C2–C3 1.570(3)

Figure 2. Thermal-ellipsoid plots of $\mathbf{2}_{Cl}$, $\mathbf{2}_{Br}$, and $\mathbf{2}_{I}$ (ellipsoid probability: 50%) and selected bond lengths [Å].

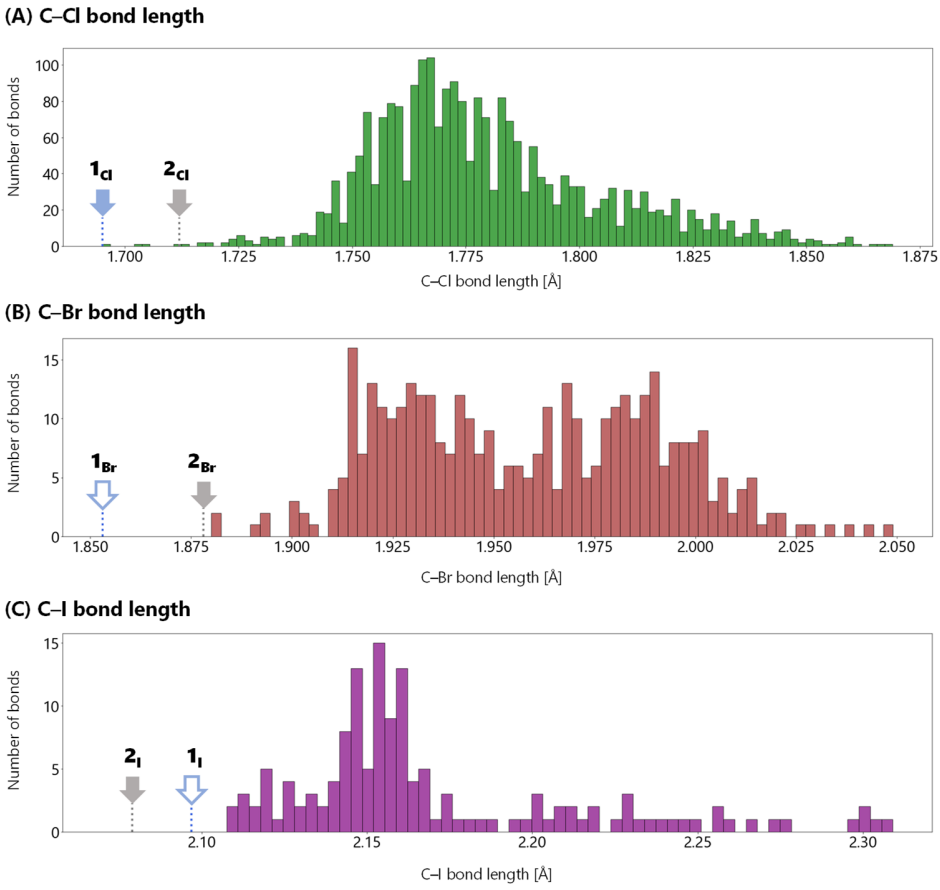

Figure 3. Distribution of the lengths of tetra-coordinated carbon–halogen bonds extracted from the CCSD. The bond lengths of **1** and **2** are indicated by arrows on the histogram. It is worth noting here that $\mathbf{1}_{Br}$ and $\mathbf{1}_{I}$ do not satisfy the criteria of these histograms due to their relatively poor data quality. These bond lengths are highlighted by white arrows with a blue outline; number of reported structures: (A) 1433 hits, (B) 321 hits, and (C) 124 hits.

Table 1. C(sp^3)–halogen bond lengths [Å] in halotrinitromethanes (1)[18,19] and hexafluorodihalocubanes (2) as determined using single-crystal X-ray diffraction (scXRD) analysis, X-ray absorption spectroscopy (XAS) in THF, gas-electron diffraction (GED) analysis, and density functional theory (DFT) calculations at the M06-2X/aug-cc-pVTZ (for C, N, O, F, and Cl) and aug-cc-pVTZ-PP (for Br and I) levels.

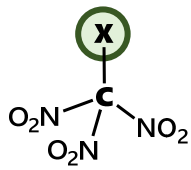

($\mathbf{1_{Cl}}$) **X** = Cl
($\mathbf{1_{Br}}$) **X** = Br
($\mathbf{1_{I}}$) **X** = I

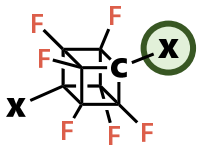

($\mathbf{2_{Cl}}$) **X** = Cl
($\mathbf{2_{Br}}$) **X** = Br
($\mathbf{2_{I}}$) **X** = I

	r (X–C)			
	scXRD	XAS	GED	DFT
$\mathbf{1_{Cl}}$	1.6944(14)	-	1.712(4)	1.701
$\mathbf{2_{Cl}}$	1.717(2)	1.722(17)	-	1.719
$\mathbf{1_{Br}}$	1.853(5)	-	1.869(6)	1.873
$\mathbf{2_{Br}}$	1.878(3)	1.876(4)	-	1.877
$\mathbf{1_{I}}$	2.097(4)	-	-	2.100
$\mathbf{2_{I}}$	2.079(3)	2.101(8)	-	2.079

In addition to the geometric parameters of a single molecule of **2**, the intermolecular interactions in the crystalline state were examined. Due to the electron-withdrawing nature of the hexafluorocubane skeleton, halogen atoms other than fluorine atoms in **2** are expected to be electron-deficient. These kinds of electron-deficient halogen atoms likely create Lewis-acidic σ-holes, which are known to participate in interactions with Lewis bases. The resulting interactions are known as halogen-bond and might significantly affect the bond lengths of C–X bonds, once a certain amount of electron density is donated to their σ* orbital.[31] Therefore, it is necessary to clarify whether halogen-bond interactions exist in the crystalline state, and if so, how the C–X bond length is influenced by the halogen-bond interaction in the crystal packing.

The representative intermolecular atomic distances and the results of Hirshfeld surface analyses[32] of **2** in the crystalline state are shown in **Figure 4A–F**. In the packing structure, short contacts between fluorine and either chlorine, bromine, or iodine below the sum of their van der Waals radii were observed, even though each of these interatomic distances was by only 0.03–0.12 Å shorter than the sum of the van der Waals radii. The C–X–F (θ_1) angles in each of these compounds are 150~160°, indicating that these contacts are induced by the halogen-centered σ-holes of the heavier halogen atoms. Moreover, the presence of bond paths and bond critical points (BCPs) with a positive value of the Laplacian of the electron density ($\nabla^2\rho_{BCP}$) between F and X in the atoms-in-molecules (AIM) analyses[33] are consistent with weak interactions at the heavier halogen atoms (**Figures S2–4**). The results of the Hirshfeld surface analysis suggest that there are interactions between the center of the cyclobutane ring and the fluorine atoms. These interactions could be categorized as non-covalent carbon-bonding interactions, which represent interactions between a Lewis acidic σ-hole centered on a carbon atom and a Lewis base; these have been described in previous studies as a characteristic type of interaction in highly fluorinated cubanes.[28,34,35] The halogen-bond and the carbon-bonding donor capabilities of **2** were examined by means of the surface-electrostatic-potentials. Geometry optimization and electron-density analyses of **2** were conducted at the M06-2X/aug-cc-pVTZ (aug-cc-pVTZ-PP for Br and I) levels, and the electrostatic potential maps and the electrostatic potentials at the σ-holes obtained from DFT calculations are shown in **Figure 4G–I**. In the electrostatic potential maps, $V_{S,max}$ represents the extremal electrostatic potential value on an electron density isosurface which is 0.001 a.u. away from the atomic centers. The σ-hole on the carbon center is denoted as $V_{S,max}$(C), and those on the halogen centers as $V_{S,max}$(X = Cl, Br, or I). The values of $V_{S,max}$ are also presented in **Figure 4**. Comparing $V_{S,max}$(C) values of **2**, the positive charge on the carbon decreases with increasing atomic number of the substituted halogen atom. This suggests that the positive charge on the carbon atom decreases with decreasing electronegativity of the substituent. On the other hand, focusing on the σ-holes on the halogen atoms, σ-holes are present in all cases of **2** and the value of $V_{S,max}$(X) increases with increasing atomic number of the halogen atom, which can be rationalized in terms of the increased polarizability of the heavier halogen atoms. Based on the above observations, chlorine, bromine, and iodine in **2** can participate in the halogen-bond interactions with the fluorine atoms in the solid state.

Subsequently, we carried out a non-covalent interaction (NCI) plot analysis[36] and a natural bond orbital (NBO) analysis[37] to clarify the strength of these intermolecular interactions (**Figure 5**; for details, see the SI). The wavefunctions used for these analyses were obtained from single-point calculations of the dimer structures of **2** whose geometries were extracted from their crystal structures; the calculations were conducted at the M06-2X/aug-cc-pVDZ (aug-cc-pVTZ for Cl, and aug-cc-pVTZ-PP for Br and I) levels. The NCI surface corresponding to a reduced gradient (RDG(s)) = 0.5 a.u. indicated halogen-bond

interactions, albeit that the sign(λ_2)ρ on the NCI surface was ~0, which indicated that these non-covalent interactions were only weakly attractive (**Figures 5A**, **S6A**, **S8A**, and **S10A**). Moreover, the scatter plot of RDG(s) as a function of sign(λ_2)ρ, which showed no significantly negative points in the region RDG < 0.5, clearly supports the absence of strongly attractive interactions (**Figures S6C**, **S8C**, and **S10C**). The NBO analysis of **2** was thus in accord with the NCI plots, given that the interaction energies associated with the electron donation to σ* orbitals of the C–X bonds were less than 0.4 kcal/mol (**Figures 5B**, and **S11–13**). Consequently, although short contacts between fluorine and the heavier halogen atoms exist, intermolecular electron donation from external fluorine atoms to the heavier halogen atoms are not significant. It can therefore be concluded that the influence of intermolecular interactions on the bond lengths are negligible in the case of **2**. In fact, the C–X bond lengths obtained from the optimized dimer structures that form halogen-bond show < 0.003 Å elongation compared to those obtained from the optimized monomeric structures of **2** in the gas phase (**Figures S5**, **S7**, and **S9**). Our discussion based on XAS results also supports this conclusion (*vide infra*).

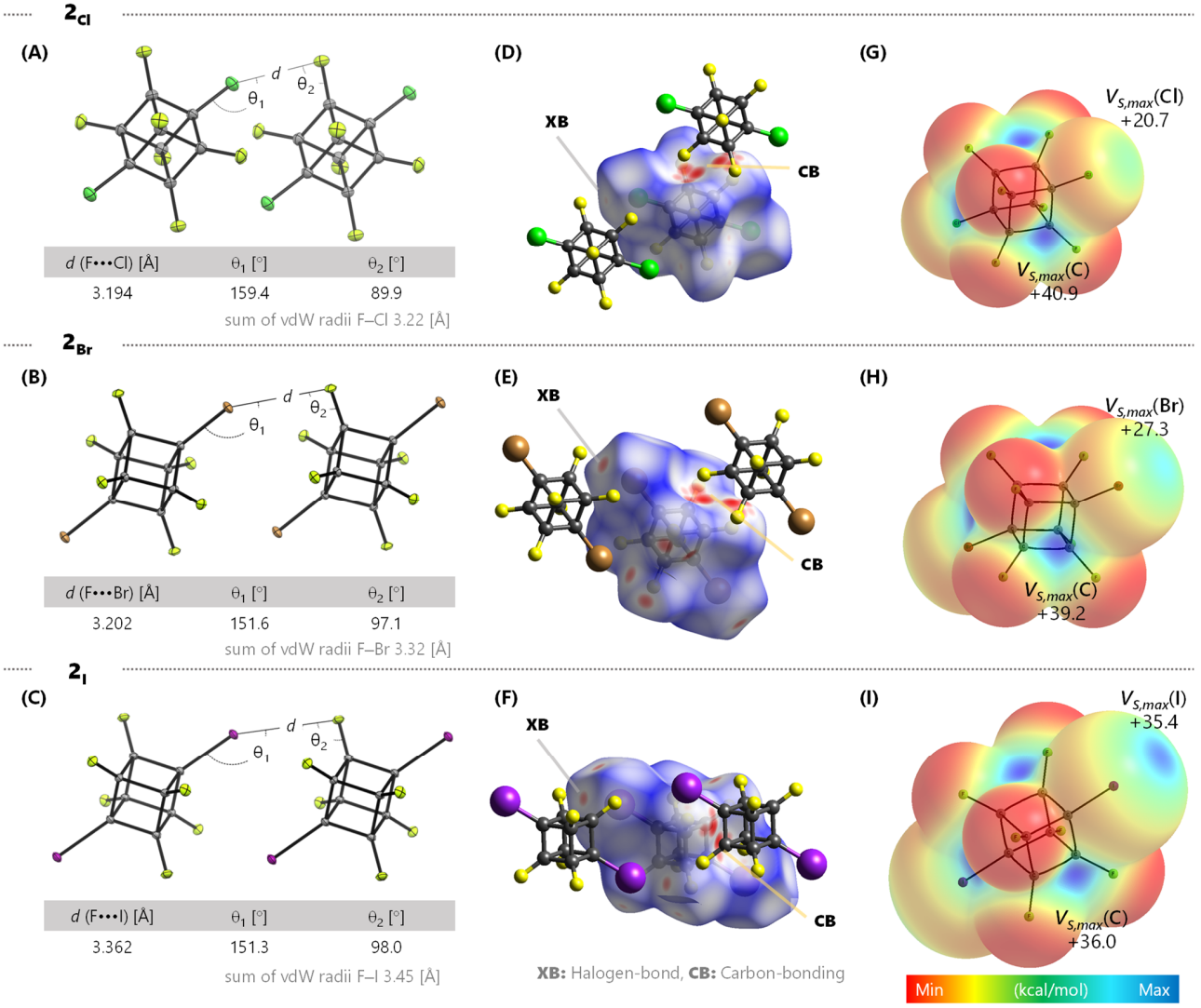

Figure 4. Packing structures of hexafluorodihalocubanes (**2**). Intermolecular F···X distance and related angles for $\mathbf{2}_{\mathbf{Cl}}$ (A), $\mathbf{2}_{\mathbf{Br}}$ (B), and $\mathbf{2}_{\mathbf{I}}$ (C) in the crystal structure. Hirshfeld surfaces for dimers of $\mathbf{2}_{\mathbf{Cl}}$ (D), $\mathbf{2}_{\mathbf{Br}}$ (E), and $\mathbf{2}_{\mathbf{I}}$ (F) in the crystal structure mapped using d_{norm}. Electrostatic-potential-surface maps and the electrostatic potentials for $\mathbf{2}_{\mathbf{Cl}}$ (G), $\mathbf{2}_{\mathbf{Br}}$ (H), and $\mathbf{2}_{\mathbf{I}}$ (I). The molecular electrostatic potentials were projected on the electron-density isosurface, which is 0.001 a.u. away from the atomic centers. The colors form a continuum from the most positive value in its potential (blue) to the most negative value in its potential (red).

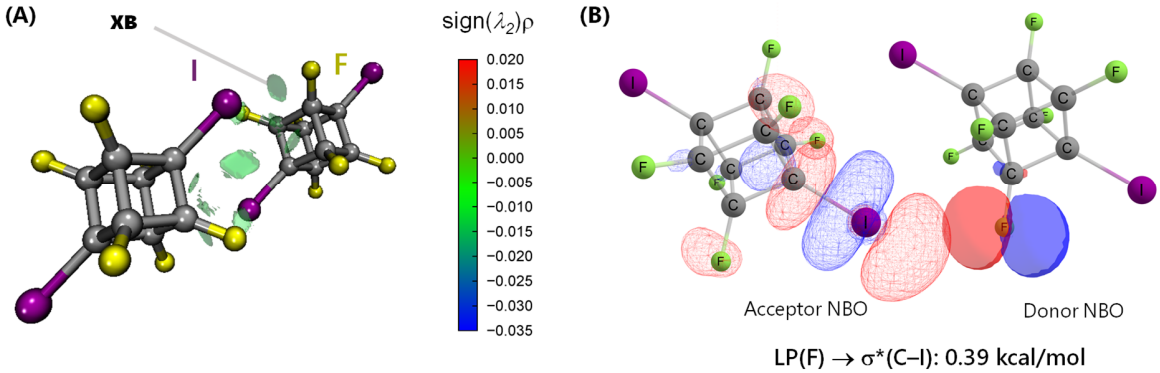

Figure 5. Quantitative evaluations of the non-covalent intermolecular interaction in $\mathbf{2_I}$. (A) Non-covalent interaction (NCI) plots of $(\mathbf{2_I})_2$ obtained from the crystal structure where cutoffs were set at RDG(s) = 0.5 a.u., and –0.05 < sign(λ_2)ρ < 0.05 a.u. The color scale ranges from –0.035 a.u. (blue) to 0.020 a.u. (red). RDG, reduced gradient; λ_2, a second eigenvalue of the electron-density Hessian matrix; ρ, electron density; XB, halogen-bond. (B) Second-order perturbation theory analysis of $(\mathbf{2_I})_2$. Each natural bond orbital (NBO) is depicted using filled surface for a donor NBO and meshed surface for an acceptor NBO. For the second-order perturbation theory analysis, only the energies and donor/acceptor NBOs corresponding to the largest interactions of $(\mathbf{2_I})_2$ are shown. The results for the other compounds and a further analysis of $(\mathbf{2_I})_2$ are provided in the SI.

X-ray absorption spectroscopy. Almost all studies on carbon–halogen bonds have been discussed based on the molecular structure obtained from scXRD and gas-electron diffraction (GED) measurements. Although solid-state structures derived from scXRD analysis are well established, this approach suffers from the potential flaw that the molecular structure may be affected by intermolecular interactions from adjacent molecules due to crystal packing, which complicates the understanding of intrinsic bond properties. While the GED method allows a more precise structural analysis of molecules, it is limited to simple gaseous molecules and requires a special electron diffractometer equipped with a jet nozzle and cold-trap accessories.[38,39] Here, we extended the scope of our research to solution systems by adopting XAS. XAS is arguably one of the most powerful techniques to unveil not only the local structure but also electronic state of the target atoms without being restricted by the state of the sample; XAS can thus provide a variety of chemical and physical information on a compound. Hence, we speculated that it should be possible to use XAS to elicit information on the C(sp^3)–X bonds of **2**, such as the bond length in solution and the electronic state of halogen, which has not been investigated so far.

Cl K-edge XAS experiments of $\mathbf{2_{Cl}}$ were performed in THF using an originally designed solution cell for tender-energy XAS measurement (**Figure S14**). An intense and sharp peak corresponding to the electric dipole transition from Cl 1s to antibonding σ* orbitals was observed at 2822 eV, which is a typical feature of the X-ray absorption near edge structure (XANES) of organochlorides (**Figure 6B**).[40,41] Time-dependent density functional theory (TDDFT) calculations on $\mathbf{2_{Cl}}$ were performed at the ZORA-B3LYP/ZORA-def2-TZVP(-f) level using the ORCA 6.0.0 program package.[42–45] The results of the TDDFT calculations showed that the main components of the first peak are associated with the Cl 1s → LUMO and LUMO+1 transitions, which possess a large Cl p contribution of 13.6% and 27.4%, respectively (**Figure S24**). Although we attempted XAS experiments in the solid state for comparison, the shape of the XANES spectra were not identical to each other in all scans due to the susceptibility of $\mathbf{2_{Cl}}$ toward sublimation (**Figure S17**). The extracted k^3-weighted extended X-ray absorption fine structure (EXAFS) oscillation was Fourier transformed between the k-range from 3.5 $Å^{-1}$ and 9.0 $Å^{-1}$. A peak derived from Cl–C1 scattering was observed at 1.4 Å, and those of Cl–C2 and Cl–F scatterings were found between 2.0–3.5 Å in the radial structure function (**Figure 6A**). The thus-obtained FT-EXAFS was fitted in the r-space (r: 0.8–3.5 Å) using three scattering paths calculated based on the geometric structures obtained from scXRD. The bond length between Cl and C1 in THF was determined to be 1.722(17) Å with a coefficient of multiple correlation factor (R factor) of 1.8% (**Tables 1** and **S2**). Although the static error was somewhat high due to the narrow k-range, the C(sp^3)–Cl bond length of $\mathbf{2_{Cl}}$ in solution was almost identical to that in the solid state determined by scXRD. This result suggests that the C(sp^3)–Cl bond length of $\mathbf{2_{Cl}}$ is not significantly affected by crystal packing. To evaluate the significance of solvent effects on the C(sp^3)–Cl stretching, theoretical calculations were carried out. The geometry optimization of the [$\mathbf{2_X}$···THF] adduct was performed at the aug-cc-pVDZ level except for the halogen atoms (aug-cc-pVTZ for Cl, aug-cc-pVTZ-PP for Br, I). The thus obtained C(sp^3)–Cl bond lengths of the THF-coordinated and non-coordinated sites were identical (1.722 Å) (**Figure 6C**). This result indicates a negligible effect of the solvent on the length of the C(sp^3)–Cl bond, which is consistent with the results of the Cl K-edge XAS experiments. The calculated length of the Cl···O bond in the [$\mathbf{2_{Cl}}$···THF] adduct (2.865 Å) was shorter than the length of the intermolecular Cl···F interaction in the crystal (3.194(1) Å). Accordingly, the influence of crystal packing on the length of the C(sp^3)–Cl bond is most likely negligible.

Next, we conducted a Br K-edge XAS analysis of $\mathbf{2_{Br}}$ using THF and toluene as solvents. Although the quality of the EXAFS oscillation in toluene was slightly worse than that in THF due to the lower solubility of $\mathbf{2_{Br}}$ in toluene, all EXAFS oscillations of $\mathbf{2_{Br}}$, including that of a solid sample, were clearly observed up into the high k region (~15 $Å^{-1}$) without damping. Moreover, these EXAFS oscillations and the corresponding FT-EXAFS were almost identical. Subsequently, the fitting analysis was conducted in a manner similar to that of $\mathbf{2_{Cl}}$, and the length of the C(sp^3)–Br bond in $\mathbf{2_{Br}}$ in THF was determined to be 1.876(4) Å, which is in good agreement with the results obtained from the scXRD analysis (**Tables 1** and **S3**, **Figure 6D**). The lengths of the C(sp^3)–Br bond of $\mathbf{2_{Br}}$ in toluene (1.868(6)

Å) and in the solid state (1.870(5) Å) were also identical within error margins, corroborating negligible effects arising from solvent and packing effects on the length of the C(sp^3)–Br bond of $\mathbf{2_{Br}}$. The XANES spectra of $\mathbf{2_{Br}}$ and *tert*-BuBr are shown in **Figure 6E**. A first peak, corresponding to the Br 1s → σ* transitions, was observed at 13473 eV in all spectra.[46] TDDFT calculation of $\mathbf{2_{Br}}$ confirmed that the destinations of the transitions were the LUMO (Br p: 19.8%) and the LUMO+1 (Br p: 36.0%), respectively (**Figure S25**). Notably, the peak intensity of $\mathbf{2_{Br}}$ was substantially higher than that of *tert*-BuBr in THF, reflecting the structural and electronic characteristics of the hexafluorocubane scaffold, i.e., a reduced degree of hyperconjugation to the σ*(C–Br) antibonding orbitals due to the absence of σ-bonds at the antiperiplanar positions relative to the C–Br bond [ω(Br–C–C–C) = 135°]. The strong electron-withdrawing ability of the fluorine atoms in $\mathbf{2_{Br}}$ can be expected to further contribute to the high peak intensity. The solvent effect was observed in XANES spectra of $\mathbf{2_{Br}}$ in contrast to the small differences in EXAFS. The peak intensity increased with decreasing coordination ability of the solvent, suggesting interactions between the σ-holes at the bromine atoms and the solvent molecules, which can be expected to increase the electron density on the bromine atoms. The length of the C(sp^3)–Br bonds of the THF-coordinated and non-coordinated sites were calculated to be 1.883 Å and 1.879 Å, respectively (**Figure 6F**). This result further corroborates the negligible effect of the solvent on the length of the C(sp^3)–Br bond, which is consistent with the results of the Br K-edge XAS experiments. The calculated length of the Br···O interaction in the [$\mathbf{2_{Br}}$···THF] adduct (2.832 Å) was shorter than the length of the intermolecular Br···F bond in the crystal (3.202(1) Å), suggesting negligible C–X···F–C interactions in the crystal.

Meanwhile, a pronounced elongation of the C(sp^3)–I bond in solution was observed for $\mathbf{2_I}$. The k^3-weighted I K-edge EXAFS oscillation of $\mathbf{2_I}$ was Fourier-transformed between the *k*-range from 3.5 $Å^{-1}$ and 12.0 $Å^{-1}$. The features of the thus obtained FT-EXAFS of $\mathbf{2_I}$ resembled those of $\mathbf{2_{Cl}}$ and $\mathbf{2_{Br}}$ (**Figure 6G**). The length of the C(sp^3)–I bond obtained from the fitting analysis (2.101(8) Å) extended that of the crystal structure by 0.022 Å (**Tables 1 and S4**). This bond extension was ascribed to the strong halogen bond between $\mathbf{2_I}$ and THF to afford the [$\mathbf{2_I}$···THF] adduct in solution. The calculated length of the C(sp^3)–I bond in the [$\mathbf{2_I}$···THF] adduct (2.091 Å) extended that of the non-coordinated C(sp^3)–I bond by 0.01 Å (**Figure 6I**), and the experimental and calculated lengths of the C(sp^3)–I bond were in good agreement. Due to the poor S/N ratio of the EXAFS oscillation of $\mathbf{2_I}$ in the solid state (*k*: ~9 $Å^{-1}$), it was not possible to analyze the C(sp^3)–I bond length in the solid state with high accuracy at this point (**Figure S22A**). In response to the change in EXAFS, the absorption edge of $\mathbf{2_I}$ in THF in the XANES spectrum was by 1.5 eV shifted to the lower-energy region compared to that in the solid state, suggesting the formation of an electron-rich organoiodide through the electron donation from the lone pair of oxygen to the σ-hole of the iodine (**Figure 6H**). *Ab initio* theoretical calculations were carried out using the FDMNES code[47] to simulate XANES spectra of $\mathbf{2_I}$ in the solid state and the [$\mathbf{2_I}$···THF] adduct. A similar peak shift was observed in the simulated spectra, indicating that the experimentally observed peak shift can be ascribed to solvation (**Figure S23**). Although it is not on direct evidence, the observed solvent effect would imply negligible intermolecular interactions in the crystal. In addition, the absorption edge of *tert*-BuI, a weaker halogen bond acceptor than $\mathbf{2_I}$, in THF appeared at the same position as that of $\mathbf{2_I}$ in the solid state, rendering the argument more certain.

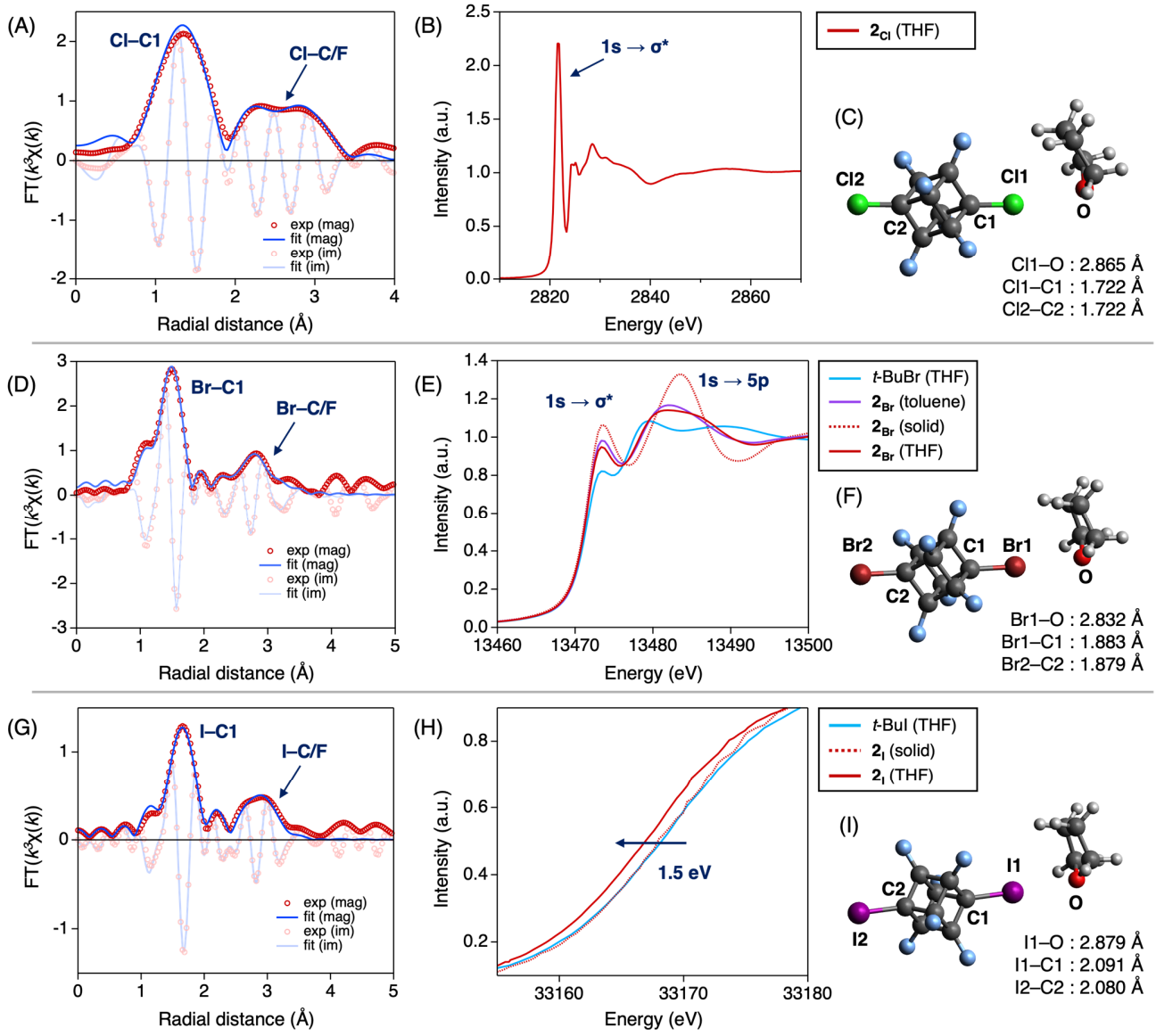

Figure 6. X-ray absorption spectroscopy of hexafluorodihalocubanes (**2**) in solution and in the solid state. (A) Cl K-edge Fourier transform-extended X-ray absorption fine structure (FT-EXAFS) of $\mathbf{2}_{Cl}$ in THF. (B) Cl K-edge X-ray absorption near edge structure (XANES) of $\mathbf{2}_{Cl}$ in THF. (C) Optimized geometry of the [$\mathbf{2}_{Cl}\cdots$THF] adduct. (D) Br K-edge FT-EXAFS of $\mathbf{2}_{Br}$ in THF. (E) Br K-edge XANES of *tert*-BuBr and $\mathbf{2}_{Br}$ in solution and in the solid state. (F) Optimized geometry of the [$\mathbf{2}_{Br}\cdots$THF] adduct. (G) I K-edge FT-EXAFS of $\mathbf{2}_{I}$ in THF. (H) I K-edge XANES of *tert*-BuI and $\mathbf{2}_{I}$ in the solid state and in THF. (I) Optimized geometry of the [$\mathbf{2}_{I}\cdots$THF] adduct; mag: magnitude; im: imaginary part.

Theoretical calculations. To obtain further insights into the bond shortening, DFT calculations of **1** and **2** were carried out. It should be noted here that the following discussion focuses solely on intramolecular effects since intermolecular effects have only negligible influences on the bond lengths, as discussed in earlier sections (*vide supra*). The optimized structures of **1** and **2** were calculated at the M06-2X/aug-cc-pVTZ (aug-cc-pVTZ-PP for Br, I) level in the gas phase, and were found to be in good agreement with the experimental structures in the solid state (**Table 1**). The wavefunctions obtained from the DFT calculations were further analyzed using NBO[37] and quantum theory of atoms-in-molecules (QTAIM)[48] calculations.

First, the s-character and double-bond character (natural bond index; NBI)[37] were investigated using the NBO program (**Figures 7A and 7B**). For both **1** and **2**, the s-character of the carbon atom in each C(sp^3)–halogen bond is higher than that associated with pure sp^3 hybridization (s-character of **1** and **2** > 25% (pure sp^3)). The high s-character is caused by the introduction of electron-withdrawing groups on the carbon atoms.[49,50] The strained cyclic skeletons of **2** may also contribute to increase in s-character.[37] Interestingly, in spite of the additional strain, the s-character of **2** is always lower than that of **1** for analogous molecules with the same halogen.

The NBI values for the C–X bonds suggest higher double-bond character for **1** than for **2** (**Figure 7B**). The double-bond

character of $\mathbf{1}_{Cl}$ corresponds to the hyperconjugation from the lone pair (LP) of the halogen to the σ* orbital of the C–N bond (**Figure 7C**; for details, see the SI), which was revealed by a second-order perturbation theory analysis.[19] Although similar hyperconjugation from the LP of the halogen to the σ*(C–C) orbital was observed for **2**, the degree of hyperconjugation was lower than that of **1**. Additionally, the higher electron occupancy of the σ*(C–N) in **1** compared to that of the σ*(C–C) in **2** is consistent with the higher double-bond character in **1**. These results indicate that the hyperconjugation and s-character of **1** both favor reduction of the C–X bond length. It is furthermore worth noting that for both **1** and **2**, the double-bond character decreases with increasing atomic number of the halogen. A second-order-perturbation-theory analysis further confirmed the reduced degree of hyperconjugation involving the σ*(C–X) orbitals in **1** and **2**, which could be another factor contributing to these exceptionally short C–X bonds (for details, see the SI). The reduced degree of hyperconjugation is consistent with the result of the Br K-edge XANES measurements of *tert*-BuBr and $\mathbf{2}_{Br}$ in solution (*vide supra*).

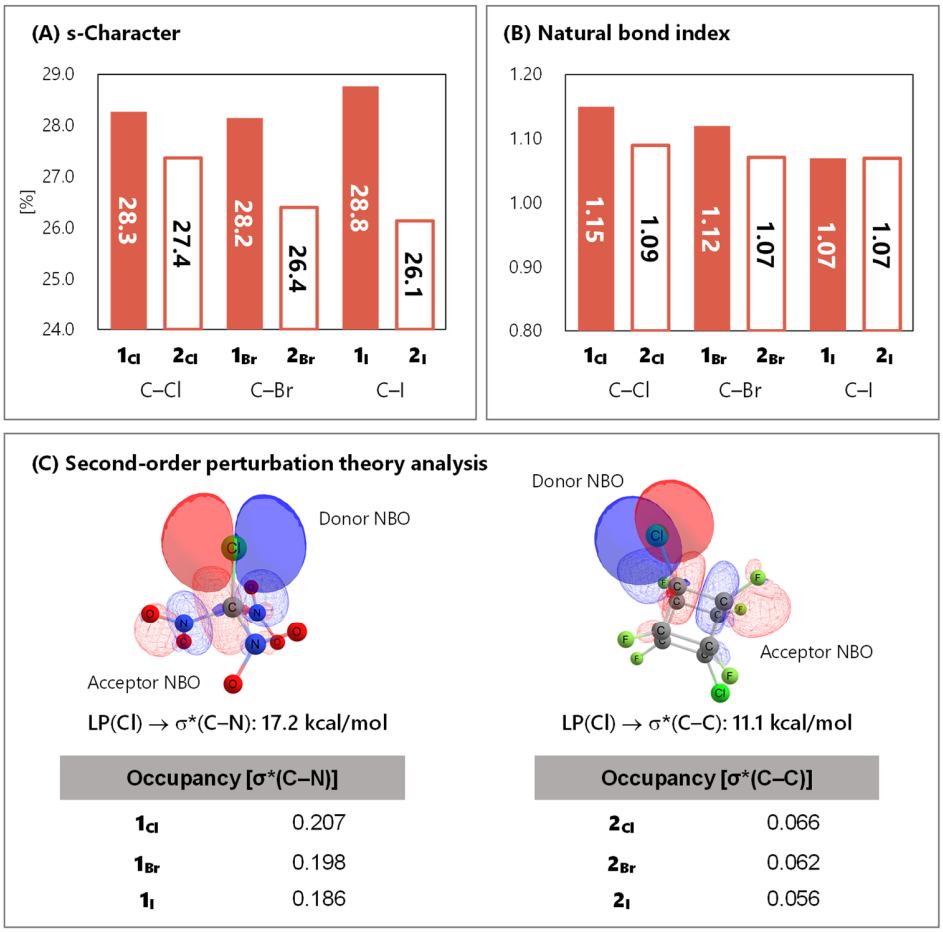

Occupancy [σ*(C–N)]	
$\mathbf{1}_{Cl}$	0.207
$\mathbf{1}_{Br}$	0.198
$\mathbf{1}_{I}$	0.186

Occupancy [σ*(C–C)]	
$\mathbf{2}_{Cl}$	0.066
$\mathbf{2}_{Br}$	0.062
$\mathbf{2}_{I}$	0.056

Figure 7. NBO analysis for the hexafluorodihalocubanes (**2**) and halotrinitrocubanes (**1**). (A) s-Character [%] of the carbon atoms that are directly bound to the (non-F) halogen atoms. (B) NBI of the C(sp^3)–halogen (non-F) bonds. (C) Second-order perturbation theory analysis of $\mathbf{1}_{Cl}$ (top left) and $\mathbf{2}_{Cl}$ (top right) together with the occupancy of the antibonding σ* orbitals (bottom). Each NBO is depicted using filled surfaces for the donor NBO and meshed surfaces for the acceptor NBO. For the second-order perturbation theory analysis, only the energies and donor/acceptor NBOs corresponding to the largest interactions of $\mathbf{1}_{Cl}$ and $\mathbf{2}_{Cl}$ are shown. The results for the other compounds and a further analysis of $\mathbf{1}_{Cl}$ and $\mathbf{2}_{Cl}$ are provided in the SI.

Next, a natural population analysis (NPA)[51] was performed in order to investigate the electrostatic effects between the bonded atoms (**Figure 8A**). In the halotrinitromethanes (**1**), both the carbon and halogen atoms were determined to be positively charged. In the hexafluorodihalocubanes (**2**), the carbon atom is negatively charged, while the halogen atom remains positively charged. Theoretically obtained electronic states of **1** and **2** were consistent with their ^{13}C NMR shifts, which is an indicator of shielding and deshielding degree around its carbon atom (**Figure 8B**). These results suggest that the Coulombic interaction between the carbon and the halogen atoms is higher for **2** than for **1**. This effect is expected to be more pronounced for heavier halogens, given that orbital interactions are significantly reduced for heavier atoms. Subsequently, we performed an interacting quantum atoms (IQA)[52] analysis. IQA is a method to analyze many-electron systems by dividing the total energy into interatomic or intraatomic terms, which clarifies the degree of attractive interaction between atoms. The interatomic-interaction energies for the carbon–halogen bonds (E_{int}(C–X)) are summarized in **Figure 8C**. The values of $\mathbf{1}_{Cl}$ and $\mathbf{2}_{Cl}$ are similar, but with increasing atomic number of the halogen, the interaction becomes more attractive for the hexafluorodihalocubanes

($\mathbf{2}_{Br}$ and $\mathbf{2}_{I}$) than for the halotrinitromethanes ($\mathbf{1}_{Br}$ and $\mathbf{1}_{I}$) when the same halogens are compared. In addition to the C–X bonds, other possible electrostatic interactions may occur between the positively charged halogens and the surrounding positively or negatively charged elements; however, these effects are less significant compared to those associated with the C–X bonds (for details, see the SI). These results indicate that the exceptionally short C–I bond in $\mathbf{2}_{I}$ is largely the result of the interatomic Coulombic interactions between the negatively charged carbon and the positively charged iodine.

Conclusion

In conclusion, we have synthesized hexafluorodihalocubanes $\mathbf{2}_{Cl}$, $\mathbf{2}_{Br}$, and $\mathbf{2}_{I}$, i.e., a new series of molecules with exceptionally short C(sp^3)–halogen bonds. The structures of $\mathbf{2}_{Cl}$, $\mathbf{2}_{Br}$, and $\mathbf{2}_{I}$ in the solid-state and in solution were exhaustively examined using single-crystal X-ray diffraction (scXRD) analysis and X-ray absorption spectroscopy (XAS). The results of these analyses also suggested that the short C(sp^3)–halogen bonds of **2** can be ascribed to intramolecular effects. Subsequently, based on a comparison using theoretical calculations with the corresponding halotrinitromethanes ($\mathbf{1}_{Cl}$, $\mathbf{1}_{Br}$, and $\mathbf{1}_{I}$), a representative family of compounds with short C(sp^3)–halogen bonds, we have comprehensively discussed the contribution of each of the intramolecular factors relevant to the bond shortening. The shortening of the C(sp^3)–halogen bonds can be explained as follows: The increased s-character of the carbon atom and the hyperconjugation from the halogen atom shorten the C(sp^3)–halogen bond. These two factors are more significant for **1** than for **2**. Interatomic Coulombic interactions between the carbon atom and the halogen atom also contribute to the bond shortening and are more significant for **2**. In the case of the compounds with smaller halogens (Cl and Br), the contributions of the s-character of the carbon atom and the hyperconjugation are dominant; therefore, the C(sp^3)–halogen bonds of **1** are shorter than those of **2**. On the other hand, for the iodine analogues, the contribution of the interatomic Coulombic interactions is dominant, and $\mathbf{2}_{I}$ has shorter C–I bonds than $\mathbf{1}_{I}$ (**Figure 9**). These results suggest that even for bonds between homologous elements (e.g., C–Cl, C–Br, and C–I), one skeleton is not always the best to form exceptionally shortened bonds. These findings can thus be expected to contribute to the challenge of reaching the "limit" of chemical bonds.

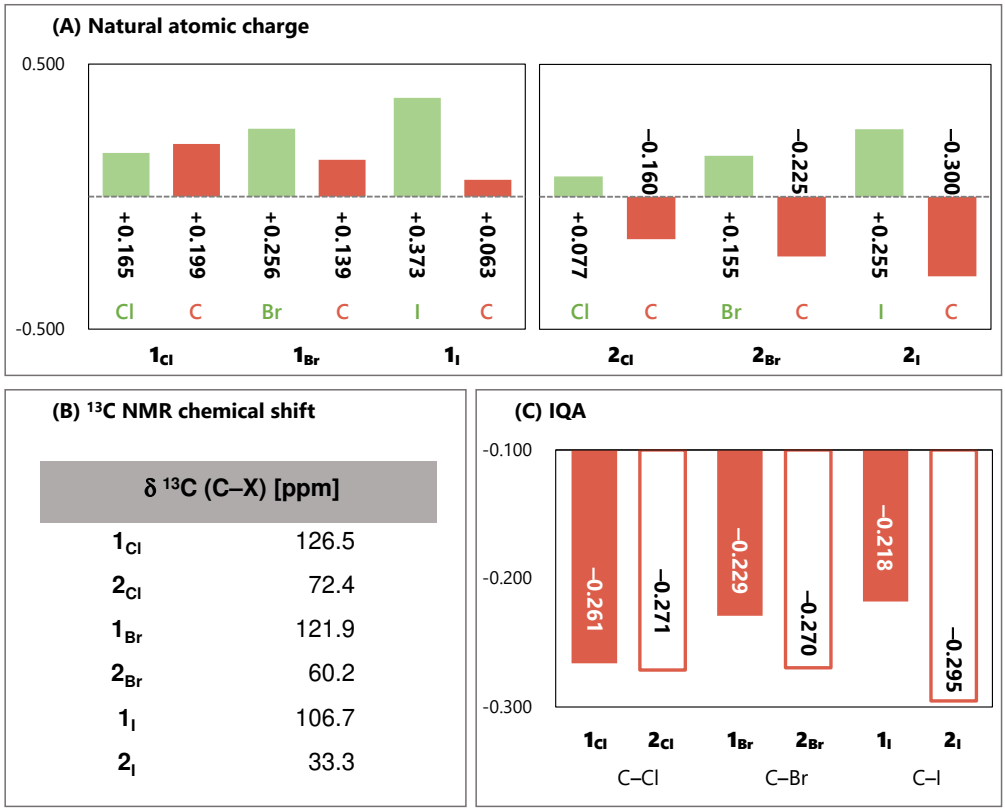

Figure 8. (A) Natural atomic charge of the carbon and halogen (Cl, Br, I) atoms. (B) Summary of the ^{13}C NMR chemical shifts of $\mathbf{1}_{Cl}$ in C_6D_6, $\mathbf{1}_{Br}$ and $\mathbf{1}_{I}$ in $CDCl_3$, and **2** in acetone-d_6. The values for **1** were obtained from refs. 18 and 19. (C) Interatomic interaction energy between carbon and halogen (Cl, Br, and I) atoms (E_{int}(C–X)). Charge values and energies are shown in atomic units.

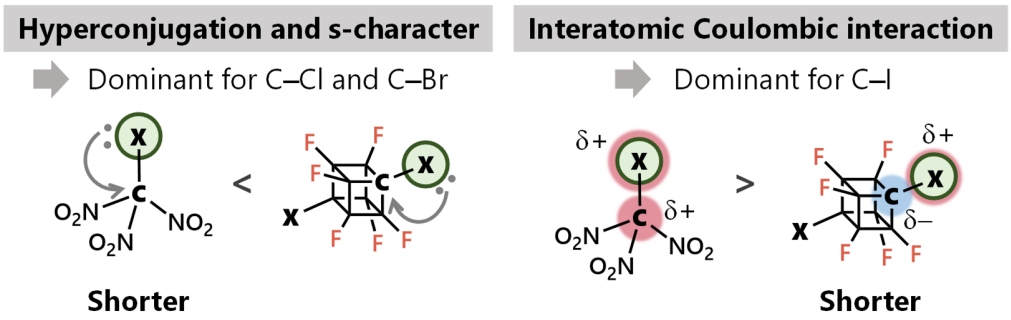

Figure 9. Schematic illustration of the dominant factors in the bond shortening for each molecule.

ASSOCIATED CONTENT

Supporting Information

The Supporting Information is available free of charge via the Internet at http://pubs.acs.org.

Detailed experimental procedures, spectroscopic data for novel compounds, details of X-ray crystallographic analyses, X-ray absorption spectroscopy, theoretical calculations, and additional discussions (PDF).

Molecular-structure file for the calculated model structures (ZIP).

Accession Codes

CCDC 2310148–2310150 contain the supplementary crystallographic data for this paper. These data can be obtained free of charge via www.ccdc.cam.ac.uk/data_request/cif, by emailing data_request@ccdc.cam.ac.uk, or by contacting The Cambridge Crystallographic Data Centre, 12 Union Road, Cambridge CB2 1EZ, UK; fax: +44 1223 336033.

AUTHOR INFORMATION

Corresponding Author

*akiyama@moleng.kyoto-u.ac.jp

*uetake@chem.eng.osaka-u.ac.jp

Funding Sources

This research was funded by AGC Inc. A part of this work was supported by JSPS KAKENHI grant JP21H05385 (to M.S.), 22K05095 (to Y.U.), 24H01851 (to Y.U.), 23K04706 (to M.A.), and 23H03950 (to M.A.); the Ito Science Foundation (to M.A.); the Inamori Foundation (to M.A.); and Yamada Science Foundation (to M.A.).

Notes

The authors declare the following competing financial interest(s): M.S., M.A., K.N., and T.O. have submitted a patent application covering the products.

ACKNOWLEDGMENT

The authors are grateful to Dr. Kohsuke Aikawa (The University of Tokyo), Dr. Ai Kohata (Tokyo Institute of Technology), Mr. Eisuke Yasuo (The University of Tokyo), and Ms. Kazumi Kohda for their help in the use of F_2 gas as well as to Dr. Kohei Watanabe (The University of Tokyo) for his help with APCI-MS measurements. The authors would also like to thank Dr. Takanori Iwasaki (The University of Tokyo), Dr. Takuya Shimajiri (Kyushu University), Prof. Shigeyoshi Sakaki (Kyoto University), and Dr. Kanami Sugiyama (Kyoto University) for helpful discussions. Moreover, the authors also thank Dr. U.F.J. Mayer at www.mayerscientificediting.com for proofreading. M.S. is grateful to the Program for Leading Graduate Schools (MERIT-WINGS) and to the JSPS for a Fellowship for Young Scientists. A part of this work was conducted in the Research Hub for Advanced Nano Characterization (The University of Tokyo), which is supported by the Ministry of Education, Culture, Sports, Science and Technology of Japan (MEXT) and in the One-stop Sharing Facility Center for Future Drug Discoveries in the Graduate School of Pharmaceutical Sciences (The University of Tokyo). XAS experiments were performed at the BL9A and NW10A beamlines of KEK under the approval of the Photon Factory Program Advisory Committee (under proposal numbers 2022G006, 2022G609, and 2024G036). Computational calculations were performed at the Research Center for Computational Science, Okazaki, Japan (under project numbers: 23-IMS-C014 and 24-IMS-C135).

REFERENCES

(1) Huntley, D. R.; Markopoulos, G.; Donovan, P. M.; Scott, L. T.; Hoffmann, R. Squeezing C–C Bonds. *Angew. Chem., Int. Ed.* **2005**, *44*, 7549–7553.

(2) Siegel, J. S. Brevity for bonds. *Nature* **2006**, *439*, 801–802.

(3) Allen, F. H.; Kennard, O.; Watson, D. G.; Brammer, L.; Orpen, A. G.; Taylor, R. Tables of Bond Lengths determined by *X*-ray and Neutron Diffraction. Part 1. Bond Lengths in Organic Compounds. *J. Chem. Soc., Perkin Trans. 2* **1987**, S1–S19.

(4) Ishigaki, Y.; Shimajiri, T.; Takeda, T.; Katoono, R.; Suzuki, T. Longest C–C Single Bond among Neutral Hydrocarbons with a Bond Length beyond 1.8 Å. *Chem* **2018**, *4*, 795–806.

(5) Uchimura, Y.; Shimajiri, T.; Ishigaki, Y.; Katoono, R.; Suzuki, T. Expandability of a long C–O bond by a scissor effect in acenaphthofuran. *Chem. Commun.* **2018**, *54*, 10300–10303.

(6) Tanaka, M.; Sekiguchi, A. Hexakis(trimethylsilyl)tetrahedranyltetrahedrane. *Angew. Chem., Int. Ed.* **2005**, *44*, 5821–5823.

(7) Frank, D.; Kozhushkov, S. I.; Labahn, T.; de Meijere, A. Cyclopropyl building blocks in organic synthesis. Part 81: Striving for unusually strained oxiranes: epoxidation of spirocyclopropanated methylenecyclopropanes. *Tetrahedron* **2002**, *58*, 7001–7007.

(8) Toda, F.; Tanaka, K.; Watanabe, M.; Tamura, K.; Miyahara, I.; Nakai, T.; Hirotsu, K. Extremely Long C–C Bond in (−)-*trans*-1,2-Di-*tert*-butyl-1,2-diphenyl- and 1,1-Di-*tert*-butyl-2,2-diphenyl-3,8-dichlorocyclobuta[*b*]naphthalenes. *J. Org. Chem.* **1999**, *64*, 3102–3105.

(9) Ishigaki, Y.; Uchimura, Y.; Shimajiri, T.; Suzuki, T. Expandability of the Covalent Bond: A New Facet Discovered in Extremely Long C_{sp3}-C_{sp3} Single Bonds. *Bull. Chem. Soc. Jpn.* **2021**, *94*, 1385–1393.

(10) Kaupp, G.; Boy, J. Overlong C–C Single Bonds. *Angew. Chem., Int. Ed.* **1997**, *36*, 48–49.

(11) Bettinger, H. F.; Schleyer, P. v. R.; Schaefer III, H. F. Tetraphenyldihydrocyclobutaarenes—what causes the extremely long 1.72 Å C–C single bond? *Chem. Commun.* **1998**, 769–770.

(12) Tanaka, K.; Takamoto, N.; Tezuka, Y.; Kato, M.; Toda, F. Preparation and structural study of naphtho- and anthrocyclobutene derivatives which have extremely long C–C bonds. *Tetrahedron* **2001**, *57*, 3761–3767.

(13) Schreiner, P. R.; Chernish, L. V.; Gunchenko, P. A.; Tikhonchuk, E. Y.; Hausmann, H.; Serafin, M.; Schlecht, S.; Dahl, J. E.

P.; Carlson, R. M. K.; Fokin, A. A. Overcoming lability of extremely long alkane carbon–carbon bonds through dispersion forces. *Nature* **2011**, *477*, 308–311.

(14) Fokin, A. A.; Chernish, L. V.; Gunchenko, P. A.; Tikhonchuk, E. Y.; Hausmann, H.; Serafin, M.; Dahl, J. E. P.; Carlson, R. M. K.; Schreiner, P. R. Stable Alkanes Containing Very Long Carbon–Carbon Bonds. *J. Am. Chem. Soc.* **2012**, *134*, 13641–13650.

(15) Fokin, A. A. Long but Strong C–C Single Bonds: Challenges for Theory. *Chem. Rec.* **2023**, e202300170.

(16) Mandal, N.; Pal, A. K.; Gain, P.; Zohaib, A.; Datta, A. Transition-State-like Planar Structures for Amine Inversion with Ultralong C–C Bonds in Diamino-*o*-carborane and Diamino-*o*-dodecahedron. *J. Am. Chem. Soc.* **2020**, *142*, 5331–5337.

(17) Li, J.; Pang, R.; Li, Z.; Lai, G.; Xiao, X.-Q.; Müller, T. Exceptionally Long C–C Single Bonds in Diamino-*o*-carborane as Induced by Negative Hyperconjugation. *Angew. Chem., Int. Ed.* **2019**, *58*, 1397–1401.

(18) Göbel, M.; Tchitchanov, B. H.; Murray, J. S.; Politzer, P.; Klapötke, T. M. Chlorotrinitromethane and its exceptionally short carbon–chlorine bond. *Nat. Chem.* **2009**, *1*, 229–235.

(19) Klapötke, T. M.; Krumm, B.; Moll, R.; Rest, S. F.; Vishnevskiy, Y. V.; Reuter, C.; Stammler, H.-G.; Mitzel, N. W. Halogenotrinitromethanes: A Combined Study in the Crystalline and Gaseous Phase and Using Quantum Chemical Methods. *Chem. – Eur. J.* **2014**, *20*, 12962–12973.

(20) Bent, H. A. Distribution of Atomic *s* Character in Molecules and Its Chemical Implications. *J. Chem. Educ.* **1960**, *37*, 616–624.

(21) Peter, L. A Continuous Quantitative Relationship between Bond Length, Bond Order, and Electronegativity for Homo and Heteronuclear Bonds. *J. Chem. Educ.* **1986**, *63*, 123–124.

(22) Wiberg, K. B. The Role of Electrostatic Effects in Organic Chemistry. *J. Chem. Educ.* **1996**, *73*, 1089–1095.

(23) Pancholi, A. K.; Iacobini, G. P.; Clarkson, G. J.; Porter, D. W.; Shipman, M. Synthesis of 4,5-Diazaspiro[2.3]hexanes and 1,2-Diazaspiro[3.3]heptanes as Hexahydropyridazine Analogues. *J. Org. Chem.* **2018**, *83*, 491–498.

(24) Lukin, K.; Li, J.; Gilardi, R.; Eaton, P. E. Stable Tin and Lead Derivatives of Nitrocubanes: Their Formation and Use in Multiple Functionalization. *Angew. Chem., Int. Ed* **1996**, *35*, 866–868.

(25) Jones, D. W.; Sunko, D. E.; Thornton-Pett, M. The Alleged Isolable 1,4,5,6-Tetrachloro-7,7-dimethoxynorbornadiene-2,3-dicarboxylic Anhydride. *J. Chem. Soc., Perkin Trans. 1* **1994**, 721–724.

(26) Wang, B.-Y.; Huang, J.-W.; Liu, L.-P.; Shi, M. Highly Efficient and Stereoselective Construction of 1-Iodo- or 1-Phenyl-selenenyl-2-aryl-3-oxabicyclo[3.1.0]hexane from the Reaction of Arylmethyl-idenecyclopropylcarbinols with Iodine or Diphenyldiselenide. *Synlett* **2005**, 421–424.

(27) Tang, D.; Gilardi, R. CCDC 177580: Experimental Crystal Structure Determination, **2002**, DOI:10.5517/cc5ysd8

(28) Sugiyama, M.; Akiyama, M.; Yonezawa, Y.; Komaguchi, K.; Higashi, M.; Nozaki, K.; Okazoe, T. Electron in a cube: Synthesis and characterization of perfluorocubane as an electron acceptor. *Science* **2022**, *377*, 756–759.

(29) Brummond, K. M.; Gesenberg, K. D. α-Chlorination of ketones using *p*-toluenesulfonyl chloride. *Tetrahedron Lett.* **1999**, *40*, 2231–2234.

(30) Dong, J.; Krasnova, L.; Finn, M. G.; Sharpless, K. B. Sulfur(VI) Fluoride Exchange (SuFEx): Another Good Reaction for Click Chemistry. *Angew. Chem., Int. Ed.* **2014**, *53*, 9430–9448.

(31) Cavallo, G.; Metrangolo, P.; Milani, R.; Pilati, T.; Priimagi, A.; Resnati, G.; Terraneo, G. The Halogen Bond. *Chem. Rev.* **2016**, *116*, 2478–2601.

(32) Spackman, M. A.; Jayatilaka, D. Hirshfeld surface analysis. *CrystEngComm* **2009**, *11*, 19–32.

(33) Bader, R. F. W. A Quantum Theory of Molecular Structure and its Applications. *Chem. Rev.* **1991**, *91*, 893–928.

(34) Frontera, A. Tetrel Bonding Interactions Involving Carbon at Work: Recent Advances in Crystal Engineering and Catalysis. *C* **2020**, *6*, 60.

(35) Bauzá, A.; Mooibroek, T. J.; Frontera, A. Influence of ring size on the strength of carbon bonding complexes between anions and perfluorocycloalkanes. *Phys. Chem. Chem. Phys.* **2014**, *16*, 19192–19197.

(36) Contreras-García, J.; Johnson, E. R.; Keinan, S.; Chaudret, R.; Piquemal, J.-P.; Beratan, D. N.; Yang, W. NCIPLOT: A Program for Plotting Noncovalent Interaction Regions. *J. Chem. Theory Comput.* **2011**, *7*, 625–632.

(37) Glendening, E. D.; Landis, C. R.; Weinhold, F. Natural bond orbital methods. *Wiley Interdiscip. Rev. Comput. Mol. Sci.* **2012**, *2*, 1–42.

(38) Berger, R. J. F.; Hoffmann, M.; Hayes, S. A.; Mitzel, N. W. An Improved Gas Electron Diffractometer – The Instrument, Data Collection, Reduction and Structure Refinement Procedures. *Z. Naturforsch., B: J. Chem. Sci.* **2009**, *64b*, 1259–1268.

(39) Reuter, C. G.; Vishnevskiy, Y. V.; Blomeyer, S.; Mitzel, N. W. Gas Electron Diffraction of Increased Performance through Optimization of Nozzle, System Design and Digital Control. *Z. Naturforsch., B: J. Chem. Sci.* **2016**, *71b*, 1–13.

(40) Smith, T. A.; DeWitt, J. G.; Hedman, B.; Hodgson, K. O. Sulfur and Chlorine K-Edge X-ray Absorption Spectroscopic Studies of Photographic Materials. *J. Am. Chem. Soc.* **1994**, *116*, 3836–3847.

(41) Myneni, S. C. B. Formation of Stable Chlorinated Hydrocarbons in Weathering Plant Material. *Science* **2002**, *295*, 1039–1041.

(42) Neese, F.; Wennmohs, F.; Becker, U.; Riplinger, C. The ORCA Quantum Chemistry Program Package. *J. Chem. Phys.* **2020**, *152*, 224108.

(43) Neese, F. Software Update: The ORCA Program System, Version 5.0. *Wiley Interdiscip. Rev.: Comput. Mol. Sci.* **2022**, *12*, e1606.

(44) DeBeer-George, S.; Petrenko, T.; Neese, F. Time-dependent density functional calculations of ligand K-edge X-ray absorption spectra. *Inorg. Chim. Acta*. **2008**, *361*, 965–972.

(45) DeBeer-George, S.; Neese, F. Calibration of Scalar Relativistic Density Functional Theory for the Calculation of Sulfur K-Edge X-ray Absorption Spectra. *Inorg. Chem.* **2010**, *49*, 1849–1853.

(46) Bergknut, M.; Persson, P.; Skyllberg, U. Molecular Characterization of Brominated Persistent Pollutants Using Extended X-ray Absorption Fine Structure (EXAFS) Spectroscopy. *Anal. Bioanal. Chem.* **2008**, *390*, 921–928.

(47) Bunău, O.; Joly, Y. Self-Consistent Aspects of X-ray Absorption Calculations. *J. Phys.: Condens. Matter* **2009**, *21*, 345501–345512.

(48) Bader, R. F. W. A Quantum Theory of Molecular Structure and its Applications. *Chem. Rev.* **1991**, *91*, 893–928.

(49) Bent, H. A. An Appraisal of Valence-bond Structures and Hybridization in Compounds of the First-row elements. *Chem. Rev.* **1961**, *61*, 275–311.

(50) Alabugin, I. V.; Bresch, S.; Gomes, G. d. P. Orbital hybridization: a key electronic factor in control of structure and reactivity *J. Phys. Org. Chem.* **2015**, *28*, 147–162.

(51) Reed, A. E.; Weinstock, R. B.; Weinhold, F. Natural population analysis. *J. Chem. Phys.* **1985**, *83*, 735–746.

(52) Blanco, M. A.; Pendás, A. M.; Francisco, E. Interacting Quantum Atoms: A Correlated Energy Decomposition Scheme Based on the Quantum Theory of Atoms in Molecules. *J. Chem. Theory Comput.* **2005**, *1*, 1096–1109.

Authors are required to submit a graphic entry for the Table of Contents (TOC) that, in conjunction with the manuscript title, should give the reader a representative idea of one of the following: A key structure, reaction, equation, concept, or theorem, etc., that is discussed in the manuscript. Consult the journal's Instructions for Authors for TOC graphic specifications.

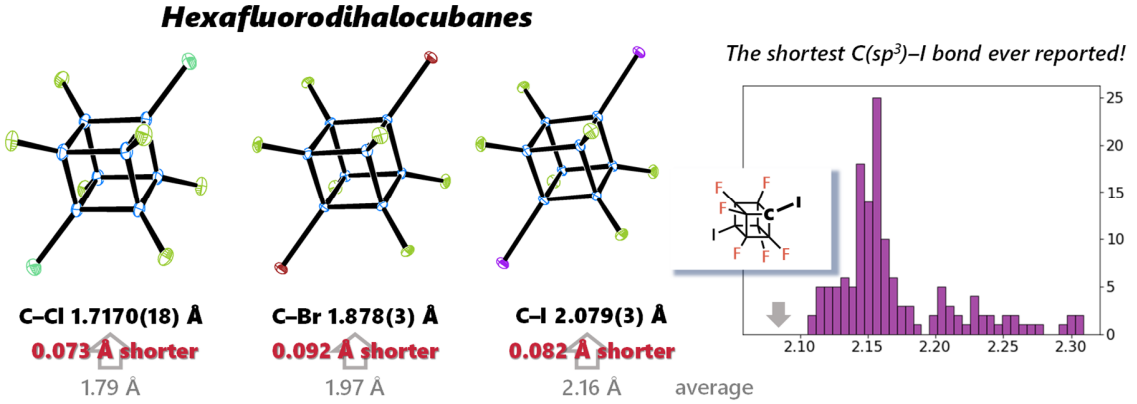

Insert Table of Contents artwork here